Optimal Voltage Regulator for Inverter Interfaced Distributed Generation Units
Part II: Application

Mohsen Eskandari, Frede Blaabjerg, *Fellow, IEEE,* Li Li, *Member, IEEE,* Mohammad Hassan Moradi,
Pierluigi Siano, *Senior Member, IEEE*

Abstract- The inverter-interfaced distributed generation (IIDG) units are operated either in grid-forming or grid-feeding modes. To this end, the inner control loops are embedded into the inverters' control system to achieve the control objectives. However, the dynamic performance of IIDG units are greatly affected by their control system and also by the grid's impedance characteristics. Optimal voltage regulator (OVR) previously has been proposed where the conventional inner loops have been replaced by the state feedback loop to compensate for the LC filter dynamics in order to achieve the desired dynamic performance. Utilizing the OVR, a universal model is proposed in this paper which is useful for both grid-feeding and grid-forming modes. Each mode of operation is achieved through impedance shaping as a feedback gain adjustment. To this end, the optimal impedance shaping for the universal model is determined based on the desired dynamic performance, control objectives and grid's impedance characteristics. Eigenvalue-analysis and simulation results prove the effectiveness of the universal model in the grid-feeding and grid-forming modes, in unbalanced and harmonic conditions as well as being able to suppress circulating, transient and fault currents in autonomous networked MGs.

Index Terms—**Inverter-interfaced distributed generation (IIDG), Microgrid (MG), Optimal impedance shaping, Voltage source inverters, Stability analysis.**

I. INTRODUCTION

THE renewable and sustainable-based distributed generation (DG) units are mostly connected to the *ac* grids via power converter-based interfaces, called inverters which in turn, has led to the development of new control strategies for voltage and frequency regulation as well as for power control purposes [1]. The microgrid (MG) concept with a hierarchical control structure has also been introduced where these novel control strategies are considered for inverter interfaced DG (IIDG) units integration [2]-[3]. Autonomous operation of MGs may improve the resiliency of the modern power systems and reduce construction cost in remote areas [4]. To this end, the inverter and its control system entitled as voltage source inverter (VSI) is seen as the most important part of MG as the VSI forms the voltage in the islanded MG to retain power quality indices within the standard levels, while delivering active and reactive power [6].

Various control strategies have been proposed for the VSI to impose the voltage in the MGs [1], [7]. The PI controller has become the most popular control method [8]. The reason is that PI controllers are extensively used in industry and electrical engineers are already familiar with their design also possible to do stability analysis etc. However, there are some issues related to grid-connected inverters and also with an isolated multi-VSIs system constituting an autonomous MG:

1. *Grid-connected mode;* since the VSI are not suitable to work in grid-feeding mode, which is intended to deliver pre-set active and reactive power when it is connected to the grid, a different control structure than VSI is needed based on current control mode, the so-called current source inverter (CSI) [1]. Switching between two modes of operation when an MG transfers to the autonomous mode, and vice versa, may cause undesirable transients [3], [9]. Besides, the CSI needs a synchronization unit, named phase-locked loop (PLL), in order to detect the voltage magnitude and phase angle of the grid [10]-[11]. The PLL, in turn, have some limitations in terms of band-width of its PI controller to deal with time delay in digital control [12] and non-minimum phase characteristics of the system [13], and also with impedance characteristics of the grid [14]-[16], which may cause some stability problems [17]-[19]. So, impedance shaping with an outer virtual impedance loop has been proposed to improve the stability of grid-connected inverters [20].

2. *Poor performance of the PI-based VSI to handle voltage regulation in unbalanced and harmonic conditions* [21]; although proportional-resonant (PR) controller is adopted to address nonlinear load condition [22], the system stability is affected by including extra PR loops for each harmonic component [23].

3. *Transient stability related to the autonomous networked MGs;* VSIs (grid-forming inverters) switch to the current limiting mode in fault situations. Adopting a current limiter in the control loop of VSIs is vital since the power electronic devices suffer from a low withstand-able current. However, the current limiter may put an autonomous networked MG into an unstable region due to different output impedance characteristics (dynamic behavior) of VSIs in current limiting mode[1] [24]-[25].

4. *Dynamic stability issues related to autonomous networked MGs;* VSIs are typically equipped with droop controller as a power control loop for power sharing and

---

[1] It has been demonstrated in the authors' previous works, as cited here, that current limiting changes the output impedance (dynamic performance) of IIDGs. Although, it is investigated in this paper, through simulation, that current limiting of VSIs destroys stability of the stand-alone and autonomous networked MGs, more investigations and mathematical workouts are needed to support the idea. The authors are currently working on the issue to prove the idea using the Lyapunov theory.

voltage regulation [26]-[29]. The X/R ratio of the power network impedance must be high enough to decouple the *f-P* and *V-Q* droop control loops, which is not true in low-voltage MGs [30]. This causes cross-coupling between droop loops and intensifies their interaction, which may lead to instability of networked MGs [31]-[32]. On the other hand, the output impedance of VSIs dominantly determines the dynamic performance and stability margin of networked MGs with a weak power network (low X/R ratio) [23], [33], while there is not enough flexibility in the output impedance shaping for PI-based VSIs [34]-[36].

5. *Reactive power sharing issue related to autonomous networked MGs;* the *V-Q* droop loop is regarded as a mean of voltage regulation to avoid reactive current from circulating among VSIs. However, the voltage drop represents an obstacle to reactive power sharing to be accurately implemented [37].

Since, the impedance shaping is the key solution to address the above issues [19]-[20], [23], [38], an optimal voltage regulator (OVR) has been proposed in the first part of the paper [39]. The OVR's control system works based on the optimal impedance shaping to achieve the desired control performance. So, in order to address such problems associated with conventional VSIs in MGs, this paper proposes the following:

- A universal model including the OVR, which works in both grid on/off modes based on impedance shaping (feedback gain adjustment), without requiring a PLL. The switching from the grid-feeding mode to the grid-forming mode is achieved through an appropriate impedance shaping, which is realized through the feedback gain adjustment and without any change in the control structure.
- Optimal impedance shape for the OVR to work in the grid-feeding (connected) mode;
- Optimum impedance shape for the OVR as a grid-forming converter to improve droop control performance in autonomous MGs with a weak power network and thereby eliminate the low-frequency oscillations instability concern. Moreover, since the high band-width current controller is not adopted in the OVR, the high-frequency, closed to switching frequency, oscillations instability concern as well as harmonic-resonant frequency oscillations [23] is also obviated;
- The control loop of the OVR to be adapted to provide fault-ride through capability (current limiting), voltage regulation in unbalanced and harmonics condition, and suppressing transient as well as circulating reactive currents.

In the next section, the universal model is introduced followed by proposing impedance shaping methods for grid-feeding and grid-forming operation modes. The OVR structure is adapted in Section III to handle unbalanced and nonlinear loads, followed by evaluating its performance in MGs, which is presented in Section IV. Simulation results are presented in Section V. Finally, conclusions are presented in Section VI.

II. A UNIVERSAL MODEL UTILIZING THE OVR

A. Control System

A universal model is proposed using the OVR to operate in both grid-forming and grid-feeding modes.
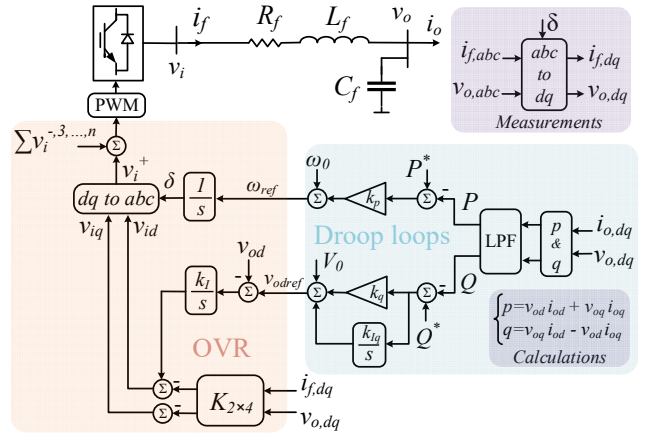

Fig. 1. The proposed universal model for both grid-forming and grid-feeding operation modes including the OVR and droop controllers as the (active and reactive) power loops. The $i_{o,dq}$ are obtained through $i_{f,dq}$ and $v_{o,dq}$ to save operating costs. The v_i^- and v_i^n are related to the negative and selected (n^{th}) harmonic loops.

To this end, the OVR is equipped with the *f-P* and *V-Q* droop loops given as follows:

$$\omega_{ref} = \omega_0 - k_p \left(P - P^* \right) \quad (1)$$

$$v_{odref} = V_0 - \left(k_q + \frac{k_I}{s} \right)\left(Q - Q^* \right) \quad (2)$$

where ω_0 and V_0 are the nominal angular frequency and voltage magnitude, respectively; ω_{ref} and v_{odref} are the references for angular frequency and voltage magnitude; k_p and k_q are the droop gains; k_I is the integrator gain for *V-Q* loop; P and Q are the average of output active and reactive power given from passing instantaneous p and q through a low-pass filter (LPF); P^*&Q^* are pre-set references for active and reactive power. The reference values (P^* and Q^*) are determined for grid-connected IIDGs. For dispatchable IIDG units, which switch to the grid-forming operation mode when the MG transfers to the autonomous mode, the reference values (P^* and Q^*) are considered zero to dispatch active and reactive power among them proportional to the assigned droop gains. The droop gains, in turn, are determined based on the available capacity of IIDG units or optimally through optimal power flow (economic dispatch). The only difference in the control system between the grid-feeding mode and grid-forming mode is the impedance shaping though the feedback gain adjustment.

A schematic diagram of the universal model, including the OVR and droop/power loops, is depicted in Fig. 1. The v_i^+, v_i^- and v_i^n (where the "*i*" subscript indicates the input signal to the PWM unit and the "*n*" superscript indicates a selected harmonic component) are the input reference voltages to the PWM unit specifying the positive sequence, negative sequence and harmonic components of the output voltage. Fig. 1 generally shows the positive sequence and the "+" superscript, which indicated the positive sequence, has been ignored throughout the manuscript for the sake of simplicity. The control loops related to the negative sequence and harmonics are demonstrated in Section III.

It will be shown later in this paper that since OVR improves stability margins of the autonomous MGs through impedance shaping, larger *V-Q* droop gains can be adopted. Thus, the integrator in the *V-Q* control loop helps to achieve accurate reactive power sharing among IIDGs in the autonomous MGs with a fully decentralized method. It is also helpful for grid-connected IIDG units to deliver reference reactive power.

B. OVR's Impedance Shaping for Grid-Forming Mode in Autonomous MGs

The OVR's dynamic model, considering its output impedance model, is developed as follows:

$$v_o = G_{OVR}(s)\, v_{odref} - Z_{odOVR}(s)\, i_{od} - Z_{oqOVR}(s)\, i_{oq} \tag{3}$$

where v_o & i_o are OVR's output voltage and current respectively, G_{OVR}, Z_{odOVR}, and Z_{odOVR} are the OVR's dynamic components participate in OVR's output impedance shaping (refer to the 1st part of the paper for details [39]). In (3), Z_{oqOVR} can be ignored due to its small value in comparison to the G_{OVR} and Z_{odOVR}. Without loss of generality, since v_o's (i_o's) direction is aligned with the v_{od} (i_{od}'s) direction, v_{odref} is represented as v_{oref} and Z_{odOVR} is regarded as the dominant output impedance of OVR and it is represented as Z_{OVR}. Thus (3) is updated as follows:

$$v_o = G_{OVR}(s)\, v_{oref} - Z_{OVR}(s)\, i_o \tag{4}$$

A block diagram of the OVR's small-signal model, given from (4), is represented in Fig. 2(a), in which the MG is modeled as an equivalent impedance seen from the OVR. The overall small-signal model of OVR and its interaction with the MG is presented in Fig. 2(b), noting that $G_{OVR}=1$. The closed loop transfer function from i_o to V_{oref} is given as:

$$\frac{i_o}{v_{odref}} = \frac{1/Z_{MG}}{1 + \dfrac{Z_{OVR}}{Z_{MG}}} \tag{5}$$

And

$$i_o = \frac{1}{Z_{MG} + Z_{OVR}} v_{oref} = \Upsilon v_{oref} \tag{6}$$

Plugging (5) into (4) results in:

$$v_o = \frac{Z_{MG}}{Z_{MG} + Z_{OVR}} v_{oref} = Z_{MG} \Upsilon v_{oref} \tag{7}$$

From (6) and having the *V-Q* droop rule in mind, it is concluded that the desired phasor of Υ should be $1\angle -90°$. The $(1/\Upsilon)$ is the equivalent impedance of the OVR output impedance and the MG impedance, seen from v_{oref}, and should be purely inductive, thus making the reactive power variation proportional to the voltage magnitude variation. This issue has been illustrated in Fig. 2(c), in which the voltage magnitude variation leads to the variation of reactive current (power).

Therefore the phasor of Z_{OVR} should be complementary part of the Z_{MG}, so that $\|Z_{MG} + Z_{OVR}\|_2 = 1$ and $\angle(Z_{MG} + Z_{OVR}) = 90$. In this way, since $|Q| \approx |v_{od} i_{oq}|$, then $\Delta Q_{OVR} \approx \Delta v_{oref}^2$, which helps implementing reactive power sharing via the *V-Q* droop loop, noting that v_{oref} is determined by droop controller. With this setting default, and from (7) we have $v_0 = (|Z_{MG}|\angle(\angle Z_{MG} - 90)) v_{oref}$. This means that the OVR's output voltage magnitude (v_o) is in a restructured form of v_{oref}, through the OVR's output impedance dynamic response, to compensate MG's equivalent impedance which is an obstacle for reactive power flow and also reactive power sharing, which is evident by referring to the reactive power flow equation through an inductive power line given by $\Delta Q \approx (\Delta V / X)$. However, modeling the equivalent model of an MG, which depends to variety of factors like voltage and power levels as well as power network topology, is beyond the scope of this paper. As a general solution, a real-time grid impedance measurement [40], can be adopted to estimate the MG equivalent impedance seen from the OVR and to tune the feedback gain matrix accordingly to achieve the desired impedance shaping.
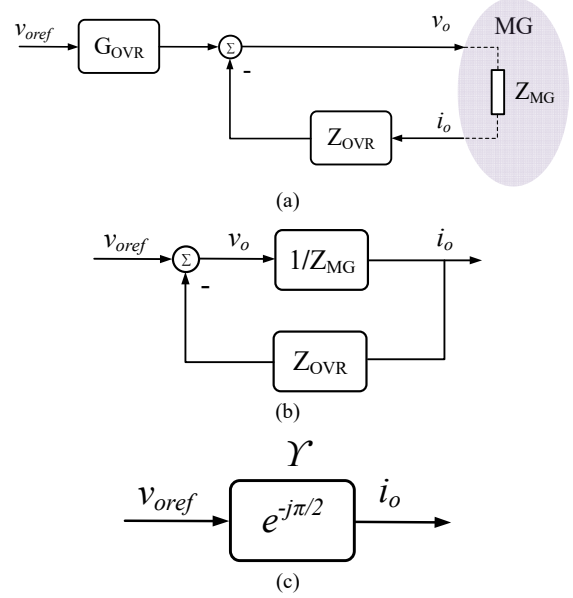

(a)

(b)

(c)

Fig. 2. The OVR model for impedance shaping as a grid-forming inverter: (a) block diagram representing small-signal model of the OVR in an autonomous MG; (b) closed-loop small-signal model including interaction of the OVR's output impedance with the MG model; (c) the equivalent model which reveals the reactive current (reactive power) variation is proportional to the voltage magnitude variation.
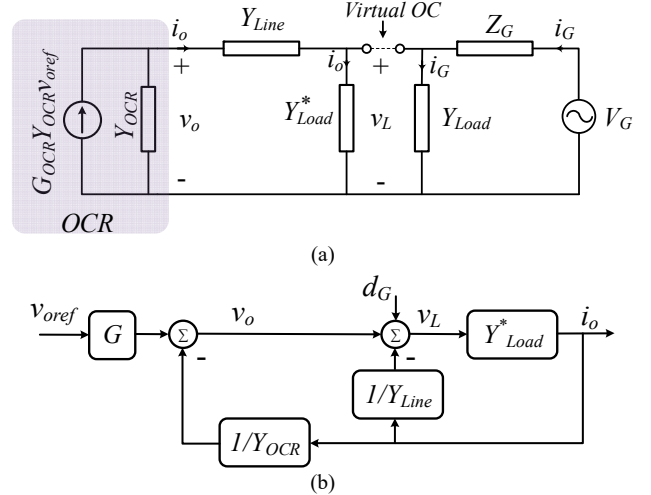

(a)

(b)

Fig. 3. The optimal current regulator (OCR) model for impedance shaping as a grid-feeding inverter: (a) electrical circuit model of OCR connected to the grid; (b) block diagram representing small-signal model of the OCR and its corresponding load (d_G represents voltage variation as a consequence of the grid voltage variation, which is inserted to the model as a disturbance).

Although it incurs computational costs, the impedance shaping is implemented adaptively to achieve real-time and optimal dynamic performance of the OVR to ensure accurate reactive power sharing and secure stability of autonomous MGs. An alternative solution, but for individual case study, only is that the X/R ratio of the power network and consequently the optimal output impedance of the OVRs can be determined by the method proposed in [33]. Since the output impedance of the OVR diffuses into the power network [33], OVR's optimal output impedance shaping helps to achieve control targets, i.e. stable and accurate power sharing. Nevertheless, as a general (off-line) solution for low-voltage MGs the desirable phasor for the output impedance of OVR is considered $1\angle 90°$ in order to satisfy the requirements mentioned earlier for Υ. Since the robustness of the OVR is guaranteed through the optimization process in the feedback gain matrix adjustment, the performance of the OVR is quite satisfactory as it is proved via the simulation results in this paper.
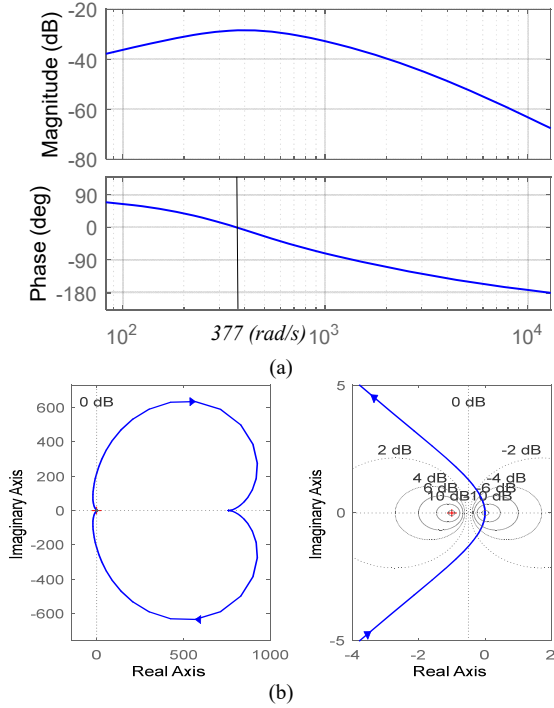
Fig. 4. Frequency response of the OCR control system in the numerical case study: (a) Bode plot of the closed loop transfer function given in (10); (b) Nyquist plot of the open loop transfer function (left plot shows full view and right plot shows zoom on (-1,0)).

C. Impedance Shaping for Grid-Feeding Mode

Grid-feeding converter are operated in the current control mode to deliver pre-set active and reactive power ($P^*\&Q^*$). So, the universal model can be called optimal current regulator (OCR) in the grid-feeding mode. In order to develop OCR's Norton model, (4) is restructured for OCR:

$$i_o = G_{OCR}(s)Y_{OCR}(s)v_{oref} - Y_{OCR}(s)v_o \qquad (8)$$

where Y_{OCR} is the OCR's output admittance. The electrical circuit for modeling the OCR connected to an **AC** grid to deliver $P^*\&Q^*$ is shown in Fig. 3 (a), where Y_{Line} is the feeder admittance which connects the OCR to the grid. The load is modeled by its admittance consisting of Y^*_{Load} corresponding to $P^*\&Q^*$ which is given by $Y^*_{Load} = V_0^2/(P^* - jQ^*)$. It is supposed that the OCR supplies Y^*_{Load} and remaining loads modeled by Y_{Load} is supplied by the grid.

So a virtual open circuit (OC) can be imagined between the OCR, including its corresponding load admittance (Y^*_{Load}), and the grid, which can be realized through the OCR's impedance shaping. The grid is modelled by a Thevenin model including voltage source (V_G) with a series impedance (Z_G). From Fig. 3(a) we have:

$$v_o - \frac{i_o}{Y_{Line}} = v_L \quad \& \quad v_L = \frac{i_o}{Y^*_{Load}} \qquad (9)$$

where v_L is the voltage across the load admittance. From (8)-(9) a block diagram representing the small-signal model of the OCR is developed as illustrated in Fig. 3(b). The closed-loop transfer function from v_{oref} to i_o is obtained as:

$$\frac{i_o}{v_{oref}} = \frac{GY_{OCR}Y_{Line}Y^*_{Load}}{Y_{OCR}Y_{Line} + Y_{OCR}Y^*_{Load} + Y_{Line}Y^*_{Load}} \qquad (10)$$

Now the problem is employing impedance shaping for the OCR to achieve the control targets, i.e. stabilizing the system and delivering $P^*\&Q^*$ with an appropriate dynamic performance. Three factors should be considered in optimal impedance shaping:
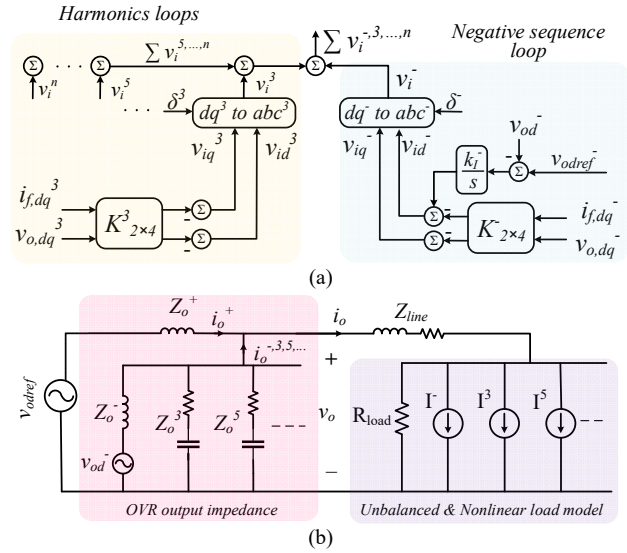

Fig. 5. Unbalanced and harmonics compensation: (a) negative sequence and harmonics control loops; (b) equivalent circuit model.

1) Based on the control system of the universal model in Fig. 1, output impedance of the OCR (Y_{OCR}) should be inductive to be consistent with *f-P* and *V-Q* droop loop and to decouple these two control loops;
2) Referring to the maximum power point tracking theory, Eq. (10) should be purely resistive;
3) A resonance should be established among Y_{OCR}, Y_{Line}, and Y^*_{Load} in order to realize virtual OC shown in Fig. 3(a) to minimize the effect of the voltage variation comes from the grid, as disturbance (d_G), on the OCR performance in delivering $P^*\&Q^*$.

In order to investigate the realization of the aforementioned factors through impedance shaping, let us consider OCR is supposed to deliver P^*=8 kW, Q^*=3 kVAr and $Z_{Line} = (1/Y_{Line}) = 0.04 + j0.188$ as a numerical case study. The desired Y_{OCR} for this case study is obtained as 0.008+j0.058 ℧, noting that $Y_{OCR}=Z_{OVR}$ (due to the duality between OVR and OCR). The desired feedback gain matrix is given as:

$$K_{OCR} = \begin{bmatrix} 133.2 & 0.02 & 326.57 & 0.07 & 842798 \\ 0.02 & 129.64 & 0.14 & 308.94 & 0 \end{bmatrix}$$

The Bode plot of (10) is shown in Fig. 4(a). The phase angle of the closed-loop transfer function at the operating frequency (ω_0=377 rad/s) is almost zero, which reveals that it is purely resistive. The maximum value of (10), which presents the equivalent admittance (minimum value for equivalent impedance), reveals that resonance occurs at the operating frequency for the specific Y^*_{Load}. It means that the virtual OC is realized to help the OCR to follow the reference values $P^*\&Q^*$. The Nyquist plot of the open loop transfer function, as shown in Fig. 4(b), proves the system stability.

III. UNBALANCED AND HARMONIC CONDITIONS

In order to make the OVR effective in unbalanced load conditions, which are quite normal at the distribution level, a negative sequence loop similar to the positive sequence loop is added to the control system of OVR. In addition, in order to provide a low impedance path for harmonic components and to make the OVR contributing in supplying the nonlinear loads, extra feedback loops are added to the OVR for each harmonic order. The control loops corresponding to the negative sequence and harmonics loops are represented in Fig. 5(a). The detailed information related to extracting the negative sequence and harmonic components of the control variables/signals can be found in

[24] and [41], respectively. The objective function, proposed in the 1st part of the paper [39], can be adapted as presented in (11) to design optimal state feedback gain matrices for the negative sequence and a selected n^{th} harmonic loops:

$$OF^{-,n} = W_1 f_1^{-,n} + W_2 f_2^{-,n} \tag{11}$$

where

$$f_1^{-,n} = w_{11} f_{11}^{-,n} + w_{12} f_{12}^{-,n} + w_{12} f_{13}^{-,n}$$

$$f_{11}^{-,n} = \left[\left\| M_G^{-,n} - abs(G_{OVR}^{-,n}) \right\|_2^2 + \left\| 0 - arg(G_{OVR}^{-,n}) \right\|_2^2 \right]$$

$$f_{12}^{-,n} = \left[\left\| M_d^{-,n} - abs(Z_{odOVR}^{-,n}) \right\|_2^2 + \left\| \phi_d^{-,n} - \frac{imag(Z_{odOVR}^{-,n})}{real(Z_{odOVR}^{-,n})} \right\|_2^2 \right]$$

$$f_{13}^{-,n} = \left[\left\| M_q^{-,n} - abs(Z_{oqOVR}^{-,n}) \right\|_2^2 + \left\| \phi_q^{-,n} - \frac{imag(Z_{oqOVR}^{-,n})}{real(Z_{oqOVR}^{-,n})} \right\|_2^2 \right]$$

$$f_2^{-,n} = \left\| G_{yu,d}^{-,n} \right\|_\infty$$

where *abs, arg, real* and *imag* denote the absolute value (magnitude), argument (phase angle), real, and imaginary parts, respectively; $\|.\|_2$ denotes 2-norm; $\|.\|_\infty$ denotes the H_∞-norm, M_G^- is the intended value for G_{OVR}^- magnitude; $M_d^{-,n}$ and $\phi_d^{-,n}$ are the intended values for $Z_{odOVR}^{-,n}$ magnitude and X/R ratio, respectively, $M_q^{-,n}$ and $\phi_q^{-,n}$ are the intended values for $Z_{oqOVR}^{-,n}$ magnitude and X/R ratio, respectively; $W_{1,\,2}$ and w_{11}, w_{12}, w_{13} are the weighting coefficients. The following modifications should be considered in developing (11):

1) ω_0 is replaced with $-\omega_0$ for the negative sequence and with $n \times \omega_0$ for the nth harmonic in developing OVR's state-space model and output impedance relevant to the negative sequence and n^{th} harmonic control loops, with the same process as given in (15)-(26) in the first part of the paper;

2) The reference value of the negative sequence voltage magnitude (v_{odref}^-) is either zero to provide a balanced voltage for local loads, or a determined reference value by the secondary controller to make OVR participated in compensating negative sequence at the point of common coupling (PCC) and improving the power quality, depending on the control strategy [42]. The impedance shaping methodology for the negative sequence is similar to the positive sequence and both the positive and negative loops should reveal the same output impedance (magnitude and X/R ratio) characteristics.

3) In the case of harmonic loops, $0 > \phi_d^n > -0.5$ to provide resistive-capacitive output impedance for harmonic currents, M_G^n is considered zero and thus the integrator is removed. M_d^n can be determined in coordination with other OVR's to achieve nonlinear power-sharing, the smaller M_d^n the larger contribution in the harmonic sharing. However, this issue requires more investigation which can be considered as an open research area.

The OVR equivalent model including extra loops for negative sequence and harmonics is presented in Fig. 5(b). By avoiding current harmonics passing through the OVR's fundamental impedance (Z_o^+) and consequent harmonic voltage drop, by providing a low impedance path for them, the total harmonic distortion (THD) of the OVR's output voltage (v_o) is improved.
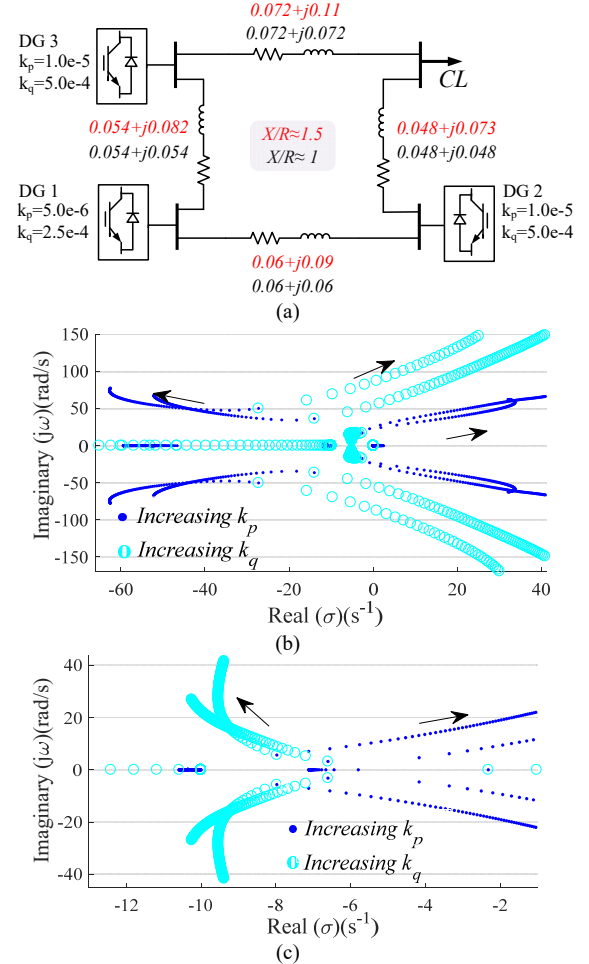

Fig. 6. Eigenvalue analysis: (a) MG topology with 3 IIDG units ($V_{L-L} = 400$ (V)); (b) dominant critical modes of the MG including VSIs; (c) dominant critical modes of the MG including OVRs. (CL: common load)

It is worth noting that including extra loops in PI-based and PR-based VSIs for harmonics and negative sequence adds four more states per loop, which makes the control system complex in terms of modelling and stability analysis, especially in modern power systems with high penetration of IIDG units. In the OVR case, only one (zero) state is added for negative sequence (harmonic) loop.

IV. OVR PERFORMANCE IN MGs

A. Stability Analysis in the Autonomous Mode

The *f-P* and *V-Q* droop control loops are included in the IIDG units' control system for power sharing and voltage regulation in the autonomous mode as follows:

$$\omega_{refi} = \omega_0 - k_{pi} P_i \tag{12}$$

$$v_{odrefi} = V_0 - k_{qi} Q_i \tag{13}$$

and the subscript *i* denotes the ith DG unit. The small-signal model of MG's power control loops including droop loops is developed as the following[2]:

$$\dot{\delta}_i = -k_{pi} P_i \tag{14}$$

$$\dot{P}_i = -\omega_c P_i + \omega_c p_i \tag{15}$$

$$\dot{Q}_i = -\omega_c Q_i + \omega_c q_i \tag{16}$$

$$\dot{\varphi}_i = v_{odrefi} - v_{odi} = V_0 - k_{qi} Q_i - v_{odi} \tag{17}$$

where δ_i is the phase angle of the ith DG unit, ω_c is the cutting frequency of LPF, and φ_i is a defined state variable of the

---

[2] Here, the integrator in the *V-Q* control loop is ignored to compare its performance with the conventional PI-based droop-based VSIs.

voltage control loop. The small-signal model of OVR is developed by updating the LC filter dynamics equations with the feedback loop (plugging (25) into (15)-(18) in the 1st part of the paper [39]). The feedback gain matrix is determined through the optimal impedance shaping rules given in Section II.B. Consequently, the small-signal model of an MG including multiple OVRs is developed by correlating the small-signal model of individual OVR through the power network. In this regard, the p and q in (15)-(16) as well as i_{od} and i_{oq} in (17)-(18) in part I are developed as a function of voltage magnitude and phase angle at the power network nodes as follows [31]:

$$\begin{bmatrix} i_{odi} \\ i_{oqi} \end{bmatrix} = \sum_{j=1}^{n} \left(\frac{\sigma_{ij}}{Z_{ij}} \left(\Gamma(-\theta_{ij}) \begin{bmatrix} v_{odi} \\ v_{oqi} \end{bmatrix} - \Gamma(\delta_{ji} - \theta_{ij}) \begin{bmatrix} v_{odj} \\ v_{oqj} \end{bmatrix} \right) \right) \quad (18)$$

$$\begin{bmatrix} p_i \\ q_i \end{bmatrix} = \sum_{j=1}^{n} \left(\frac{\sigma_{ij}}{Z_{ij}} \begin{bmatrix} v_{odi} & v_{oqi} \\ v_{oqi} & -v_{odi} \end{bmatrix} \left(\Gamma(-\theta_{ij}) \begin{bmatrix} v_{odi} \\ v_{oqi} \end{bmatrix} - \Gamma(\delta_{ji} - \theta_{ij}) \begin{bmatrix} v_{odj} \\ v_{oqj} \end{bmatrix} \right) \right) \quad (19)$$

$$\Gamma(.) = \begin{bmatrix} cos(.) & -sin(.); & sin(.) & cos(.) \end{bmatrix}$$

where θ_{ij} and Z_{ij} are phase angle and magnitude of the ij^{th} interconnecting power line, σ_{ij} is the ij^{th} entry of the power network adjacency matrix, which is 1 if DG i is connected to DG j or 0 otherwise, and n is the number of generation units in the MG. The dominant critical modes of an MG with OVRs is compared with the MG with PI-based VSIs in Fig. 6. The small-signal model of MG with VSIs is given from [31]. There are two distinct features of the critical modes of MG including VSIs and OVRs: 1) The oscillation frequency in OVR-based MGs is lower with higher damping factor; 2) Increasing V-Q droop gain of OVRs-based MG pushes the critical modes to the right-side, which is in contrast to VSI-based MG, thanks to the optimal impedance shaping of OVRs.

B. Reactive power sharing

As per stability analysis, a larger V-Q droop gain can be adopted to improve reactive power sharing, which is not applicable to VSI-based MGs due to stability issues. Since a larger droop gain improves the reactive power sharing, the integrator term of reactive power helps to achieve accurate reactive power sharing in the autonomous mode. The following modified V-Q droop loop is adopted for further improvement of the reactive power sharing and voltage regulation in OVR-based MGs:

$$v_{odrefi} = V_0 - \left(k_{qi} + \frac{k_{Iqi}}{s} \right) Q_i + \frac{k_{vi}}{s} (V_0 - v_{odi}) \quad (20)$$

where k_v is the gain of the voltage restoration loop. The third term at the right-hand side of (20), i.e. the voltage restoration term, is included to keep the voltage closed to the nominal band.

V. SIMULATION RESULTS

In this section, effectiveness of the proposed universal model is evaluated via numerical simulation in MATLAB/Simulink and the Simscape toolbox. The assessment practice includes current regulation, unbalanced/harmonic/fault conditions, power sharing and circulating reactive current. The last three items are tests in the low-voltage MG platform ($V_{L-L} = 400$ (V)) represented in Fig. 6(a). The electrical parameters and converter characteristics are same as those used in the first part of the paper [39]. The control parameters of VSI are taken from [8], which are developed to get the best dynamic performance.
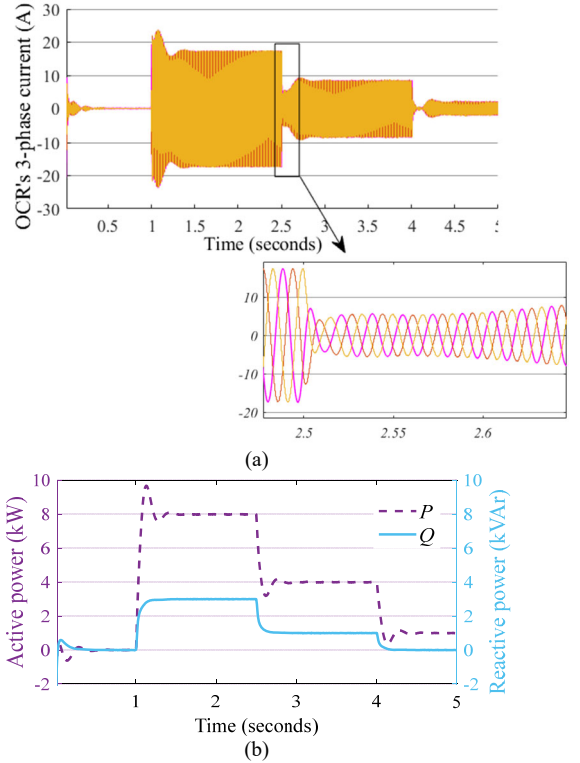
(a)

(b)

Fig. 7. OCR performance under current regulation: (a) three-phase current; (b) active and reactive power.
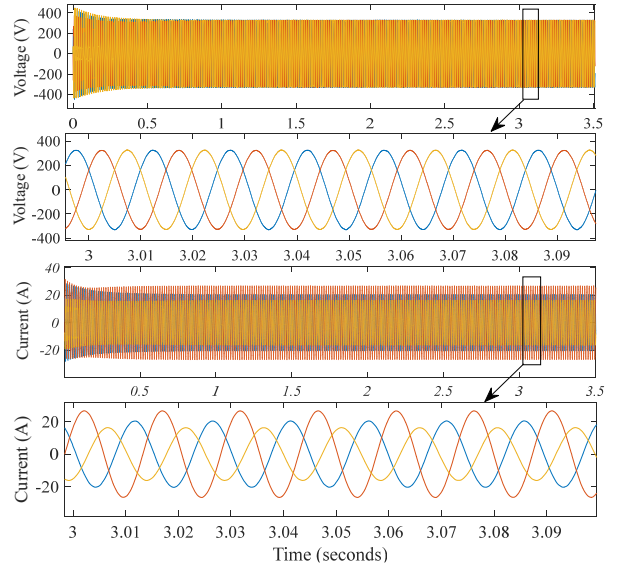
Fig. 8. OVR performance under the unbalanced condition.

A. Grid-feeding mode (OCR)

The universal model is connected to a grid via a feeder (Z_{line}=0.040+j0.188) and is operated as OCR through feedback gain adjustment. The feedback gain matrix for the OCR is determined by the optimal impedance shaping rule presented in Section II.C. The performance of OCR in current regulation is depicted in Fig. 7. The OCR is connected to the grid at $t = 0$ (s) with putting $P^* = 0$ and $Q^* = 0$ to synchronize the inverter with the grid. The following changes are applied to the universal model to check if the model follows the reference values: $P^* = 8\ kW$ and $Q^* = 3\ kVAr$ at t = 1 (s); $P^* = 4\ kW$ and $Q^* = 1\ kVAr$ at t = 2.5 (s); $P^* = 1\ kW$ and $Q^* = 0$ at t = 4 (s). The inverter follows the reference values with appropriate dynamics. Also, the system is robust in a variety of operating points thanks to the objective function proposed in the 1st part of the paper.
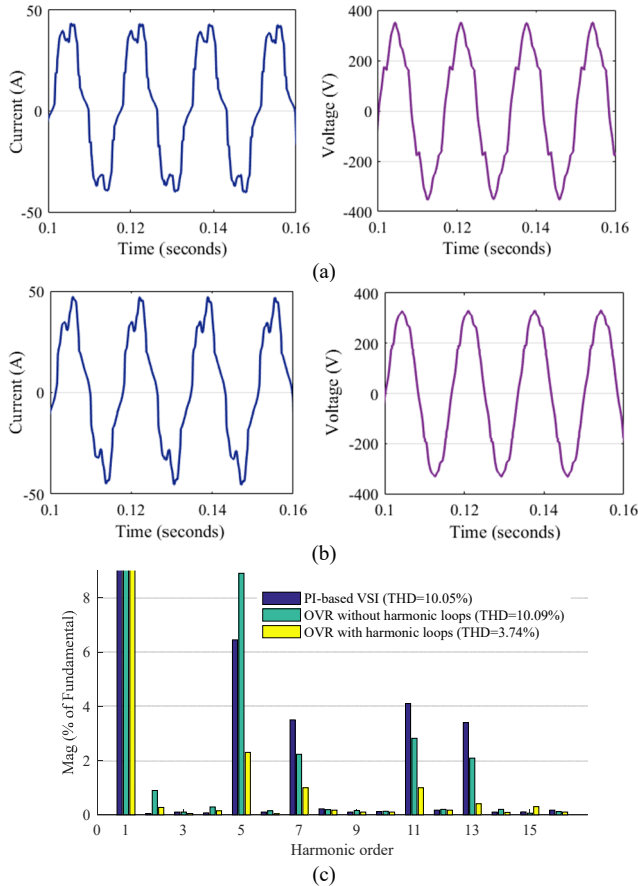
Fig. 9. OVR performance in presence of nonlinear loads: (a) OVR performance without harmonic loops; (b) OVR performance with harmonic loops; (c) THD of the voltage at PCC.

B. OVR performance in autonomous MGs

Unbalanced condition: Simulation results for unbalanced condition is shown in Fig. 8. Although the output current is unbalanced, the output voltage is balanced. The unbalanced condition imposes alternating components (with a frequency twice the nominal frequency) into *d-q* components. The *d-q* components of the negative sequence are given from Park transformation matrix with $(-\omega_0)$ and notch filter to filter out the oscillating terms.

Harmonics: a diode rectifier (with 1mH+25Ω‖50µF as DC load) is adopted to model a nonlinear load at PCC (including (6+*j*3) kVA as linear load). The simulation result is depicted in Fig. 9. The OVR with harmonics loops provides a path for harmonic current (the current in Fig. 9(b) is more distorted than that in Fig. 9(a)). As a result, the voltage in Fig. 9(b) become less distorted and the power quality at the PCC is improved. Fig. 9(c) reveals that the THD of voltage at the PCC is significantly improved from 10.1% for OVR without harmonic loops to 3.7% for OVR using harmonic loops. This improvement is achieved with including feedback loops without adding any extra state to the control system, thanks to the harmonics loops and the impedance shaping method to make the output impedance of the OVR resistive-capacitive for the harmonic loop.

Transients and Stability: in order to evaluate the performance of the universal model in autonomous MGs, the MG depicted in Fig. 6(a) is simulated. The capacity of DG 1 is considered twice as those of DGs 2&3. So, the assigned droop gains of DG 1 is half of those for DGs 2&3. The meshed topology with direct connection of DG units in low voltage distribution grid, which reduces the stability margin of droop-based MG due to cross-coupling interaction of droop controllers [31], is considered. The poor dynamic response of the conventional VSIs as well as low X/R ratio

of interconnecting power lines (X/R=1) make the VSI-based MGs unstable as shown in Fig. 10(a). In contrast, not only the OVR-based MG is stable for the same condition (X/R=1), Fig. 10 (d), the dynamic performance is greatly improved as well, as indicated in Figs. 10(e)-(f). This statement can be confirmed by comparing the dynamic response of OVR-based MG with that of the VSI-based MG as shown in Figs. 10; although the X/R ratio is higher (X/R=1.5), the dynamic response of VSI-based MG is much more oscillatory. It also is consistent with eigen-analysis conducted in Fig. 6. It shows that in low voltage MGs, where X/R ratio is a major problem [31], the OVR can be used to address this issue. OVR suppresses the large transients and improves the dynamic stability.

Reactive power sharing and circulating reactive current: active power sharing is implemented accurately by both VSIs and OVRs according to the assigned droop gains. Nevertheless, stability margin and dynamic performance of OVR-based MG is significantly improved compared to those of VSI-based MG. The reactive power sharing is also implemented accurately by adopting universal model including the OVR. To this end, the *V-Q* droop gains of OVRs are selected 5 times larger than that of VSIs and time constant of the integrator term of *Q* is considered the same as that for integrator term in the voltage restoration term. It is worth to note that adopting large droop gains is not applicable for VSIs, which already poses poor dynamic performance and narrow stability margin even with small droop gains. To evaluate the effectiveness of the OVR in suppressing circulating current, the reactive power demanded by loads is considered to be zero. Fig. 11(a) reveals large circulating reactive power among VSIs, while Fig. 11(c) shows that circulating reactive power is significantly suppressed by the proposed OVRs. The OVRs provide only reactive power losses due to active power flow through the power lines.

Fault conditions and current limiting: in order to assess the OVR performance in current limiting mode and its effect on the stability of MGs, a fault condition is simulated. To this end, a balanced 3-phase to ground fault (with a fault resistance of 1Ω) is located in the middle of power line which connects DG 1 to DG 2, in Fig. 6(a). The fault occurs at t=1.2 s and its duration is 50 *ms*. The simulation result is depicted in Fig. 12. Switching the operating mode of PI-based VSIs to current limiting mode makes the MG unstable. The same situation can be imagined for large disturbances like severe load changes. The justification is that the current limiting leads to a voltage drop at VSI's output voltage and magnitude of the voltage drop at the individual VSIs depends on the allocations of VSIs and disturbance/fault. This, in turn, causes circulating active and reactive current with high magnitude among VSIs, noting that VSIs show variable output impedance behavior at the current limiting mode depending on the circulating currents [25], [39]. Consequently, the droop controllers change the operating points of VSIs to new points with different voltages and frequencies, particularly when the source of disturbance, e.g. a fault, is removed. The droop controllers cannot recover themselves and high circulating currents still exist, which lead to instability of the networked MG. On the other hand, OVR not only appropriately limits fault current, to protect semiconductor switches, it also makes the MG stable after fault/large disturbance condition. The argument is that the OVR preserves inductivity of its output impedance to keep the droop loops decoupled in the current limiting mode. Also, OVRs provide sufficient damping through the state feedback loop to stabilize the faulted MG.
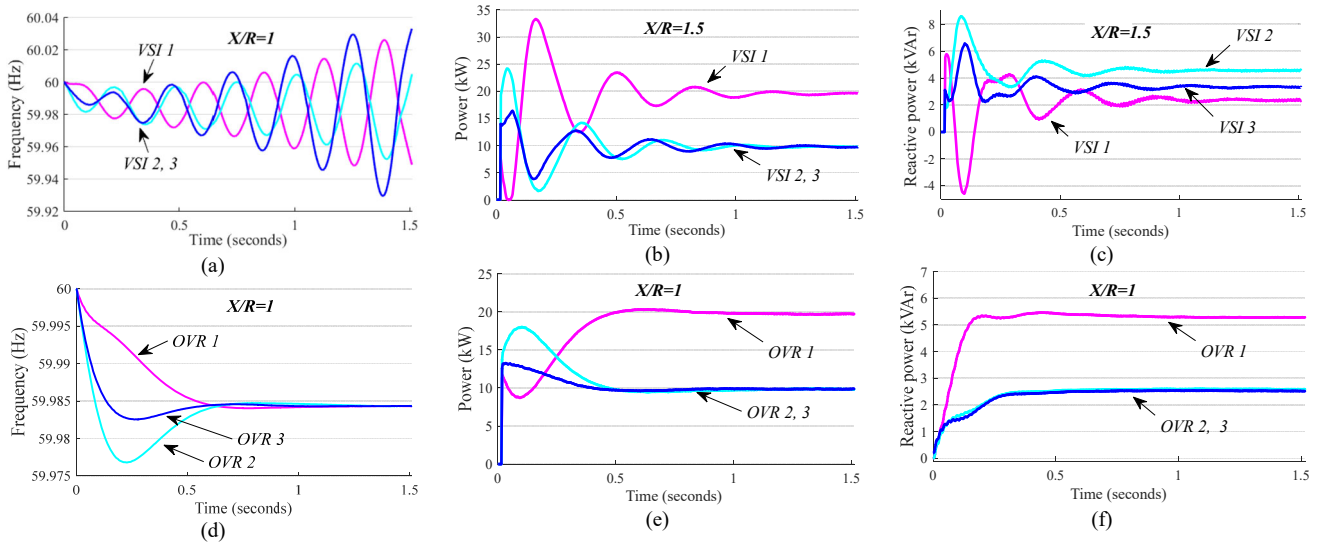
Fig. 10. OVR performance in MGs with conventional droop controller: (a) frequency of MG with PI-based VSIs and X/R=1, the system is unstable; (b), (c) dynamic response of MG, including PI-based VSIs, to P and Q sharing, X/R=1.5; (d) frequency of MG with OVRs and X/R=1, the system is stable; (e), (f) dynamic response of OVR-based MG to P and Q sharing, X/R=1. (The PI-based VSIs are marked with VSI for the sake of simplicity)
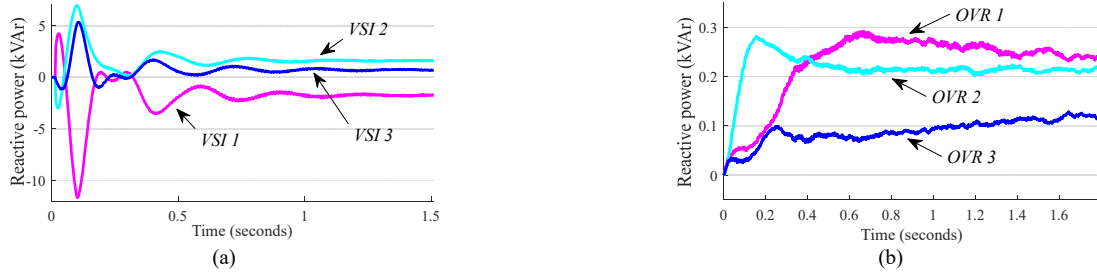

Fig. 11. Circulating reactive power: (a) among PI-based VSIs; (b) suppressed circulating reactive power among OVRs.
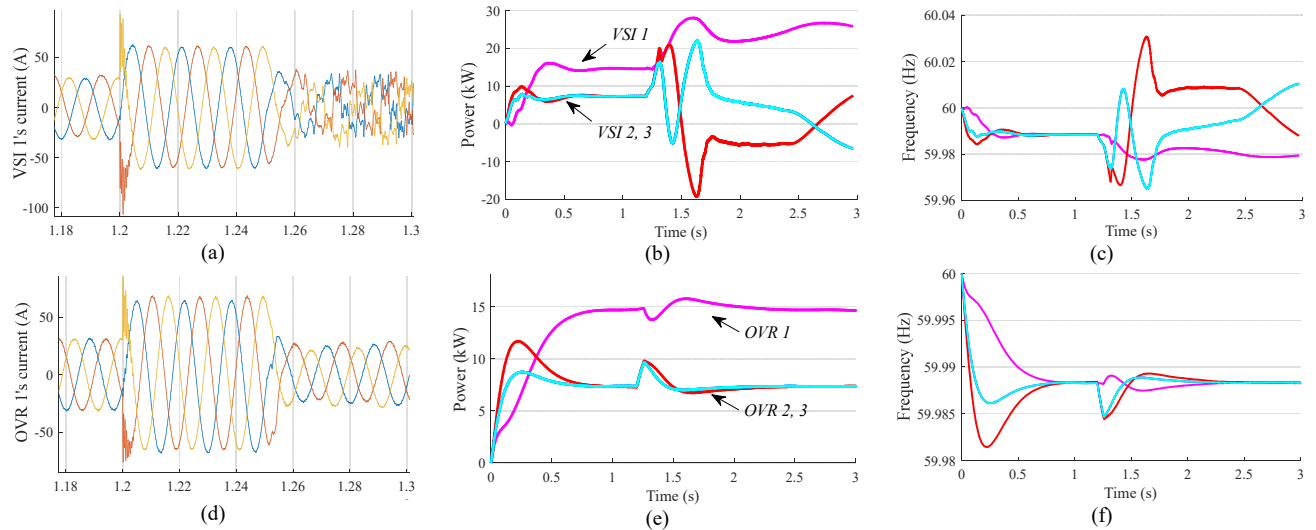

Fig. 12. Fault condition in the autonomous MG, (a)-(c) plots are related to the MG with PI-based VSIs and (d)-(f) plots related to the MG with OVRs: (a) current waveform of VSI 1; (b) active power sharing among VSIs; (c) VSIs' frequency; (d) current waveform of OVR 1; (e) active power sharing among OVRs; (f) OVRs' frequency.

VI. DISCUSSION

The impedance shaping has been considered as criteria for specifying the desired dynamic performance of IIDG unit. In this regard, the output impedance of IIDG units are controlled according to the control targets as well as the system requirement (power system characteristics) which is affected by the power network impedance and loads impedances. Loads dynamics are directly affecting the grid impedance seen from IIDG units and thus are effective in optimal impedance shaping of IIDG units.

The control challenges related to the proposed control system consist of adaptive impedance shaping and real-time (on-line) feedback gain adjustment, for further improvement of the dynamic response/stability margin of the power systems. The adaptive adjustment of the output impedance can be used to take the grid reconfigurations and load variations/dynamics into account. To realize the adaptive impedance shaping, the grid impedance seen from OVR should be monitored continuously and then the OVR's output impedance should be adjusted accordingly. In addition, adaptive impedance shaping can be helpful to achieve smooth transients from grid-connected mode to

autonomous mode. Advanced control methods like adaptive control, feedback linearization and/or sliding mode control can be adopted in this regard. In particular, as the OVR control system is based on state feedback control adopting the advanced control methods for adaptive gain adjustment is straightforward. Also, since the order of the proposed model is considerably lower than the conventional PI-based VSIs, the presented state-space model can be used in the synthesis of advanced controllers.

Nevertheless, it should be noted that the fixed optimal output impedances, designed in the second part of the paper for grid-connected mode and grid forming mode, reveal significant improvement in OVR/OCR dynamic performance in comparison to the conventional PI-based VSIs. This significant achievement is due to the proposed objective function which improves the robustness of the control system.

VII. CONCLUSION

In this paper, a universal model has been proposed for IIDG units utilizing the OVR as voltage source powered by droop control loops. Voltage regulation capability while delivering pre-set active and reactive power is a significant advantage of the universal model which is achieved by the use of impedance shaping. Optimal impedance shaping for both grid-feeding and grid-forming modes have been designed considering the desired dynamic performance, control objectives and grid impedance characteristics.

In case of MG application, the OVR improves the stability margin of droop-based autonomous MGs in both normal operation and unbalanced/harmonics/fault conditions. The precise reactive power sharing is achieved in a MG without using communication links or other signal injecting and computational-based methods.

Although robustness of the system for disturbance rejection in a variety of operating points has been considered in the feedback gain adjustment (in the optimization process in the 1st part of the paper [39]), still the real-time optimal impedance shaping remains an open topic. This issue is challenging since the grid topology, in the distribution level, may change randomly and frequently due to the power network reconfigurations and load dynamics, thus optimal impedance shaping of IIDG units should be adaptively adjusted.

REFERENCES

[1] J. Rocabert, A. Luna, F. Blaabjerg, and P. Rodriguez, "Control of power converters in AC microgrids," *IEEE Trans. on Power Electron.*, vol. 27, no. 11, pp. 4734-4749, 2012.

[2] M. H. Moradi, M. Eskandari, and H. Showkati, "A hybrid method for simultaneous optimization of DG capacity and operational strategy in microgrids utilizing renewable energy resources," *Int. J. Electr. Power Energy Syst.*, vol. 56, pp. 241-258, 2014.

[3] M. H. Moradi, M. Eskandari, and S. M. Hosseinian, "Cooperative control strategy of energy storage systems and micro sources for stabilizing microgrids in different operation modes," *Int. J. Electr. Power Energy Syst.*, vol. 6, pp. 390–400, Jun. 2016.

[4] M. H. Moradi, M. Eskandari, and S. M. Hosseinian, "Operational strategy optimization in an optimal sized smart microgrid," *IEEE Trans. on Smart Grid,* vol. 6, no. 3, pp. 1087-1095, 2015.

[5] J. M. Guerrero, J. C. Vasquez, J. Matas, L. G. De Vicuña, and M. Castilla, "Hierarchical control of droop-controlled AC and DC microgrids—A general approach toward standardization," *IEEE Trans. on Power Electron.*, vol. 58, no. 1, pp. 158-172, 2011.

[6] J. M. Guerrero, M. Chandorkar, T.-L. Lee, and P. C. Loh, "Advanced control architectures for intelligent microgrids—Part I: Decentralized and hierarchical control," *IEEE Trans. on Ind. Electron.*, vol. 60, no. 4, pp. 1254-1262, 2012.

[7] C. Buccella, C. Cecati, and H. Latafat, "Digital control of power converters—A survey," *IEEE Trans. on Ind. Inform.*, vol. 8, no. 3, pp. 437-447, 2012.

[8] N. Pogaku, M. Prodanovic, and T. C. Green, "Modeling, analysis and testing of autonomous operation of an inverter-based microgrid," *IEEE Trans. on Power Electron.*, vol. 22, no. 2, pp. 613-625, 2007.

[9] Z. Liu and J. Liu, "Indirect current control based seamless transfer of three-phase inverter in distributed generation," *IEEE Trans. on Power Electron.*, vol. 29, no. 7, pp. 3368-3383, 2013.

[10] F. Blaabjerg, R. Teodorescu, M. Liserre, and A. V. Timbus, "Overview of control and grid synchronization for distributed power generation systems," *IEEE Trans. on Ind. Electron.*, vol. 53, no. 5, pp. 1398-1409, 2006.

[11] A. Timbus, M. Liserre, R. Teodorescu, P. Rodriguez, and F. Blaabjerg. "Evaluation of current controllers for distributed power generation systems." *IEEE Trans. on Power Electron.*, vol. 24, no. 3, 654-664, 2009.

[12] J. Yin, S. Duan, and B. Liu, "Stability analysis of grid-connected inverter with LCL filter adopting a digital single-loop controller with inherent damping characteristic," *IEEE Trans. Ind. Inform.*, vol. 9, no. 2, pp. 1104–1112, May 2013.

[13] D. Lu, X. Wang, and F. Blaabjerg, "Impedance-based analysis of DC-link voltage dynamics in voltage-source converters," *IEEE Trans. on Power Electron.*, vol. 34, no. 4, pp. 3973-3985, 2019.

[14] X. Li, J. Fang, Y. Tang, X. Wu and Y. Geng, "Capacitor-Voltage Feedforward With Full Delay Compensation to Improve Weak Grids Adaptability of LCL-Filtered Grid-Connected Converters for Distributed Generation Systems," *IEEE Trans. Power Electron.*, vol. 33, no. 1, pp. 749-764, Jan. 2018.

[15] M. Davari and Y. A.-R. I. Mohamed, "Robust vector control of a very weak-grid-connected voltage-source converter considering the phase-locked loop dynamics," *IEEE Trans. on Power Electron.*, vol. 32, no. 2, pp. 977-994, 2016.

[16] D. Dong, B. Wen, D. Boroyevich, P. Mattavelli, and Y. Xue, "Analysis of phase-locked loop low-frequency stability in three-phase grid-connected power converters considering impedance interactions," *IEEE Trans. on Ind. Electron.*, vol. 62, no. 1, pp. 310-321, 2014.

[17] B. Wen, D. Boroyevich, R. Burgos, P. Mattavelli, and Z. Shen, "Analysis of D-Q small-signal impedance of grid-tied inverters," *IEEE Trans. Power Electron.*, vol. 31, no. 1, pp. 675–687, Jan. 2016.

[18] B. Wen, D. Dong, D. Boroyevich, R. Burgos, P. Mattavelli, and Z. Shen, "Impedance-based analysis of grid-synchronization stability for three-phase paralleled converters," *IEEE Trans. on Power Electron.*, vol. 31, no. 1, pp. 26-38, 2015.

[19] X. Wang, L. Harnefors, and F. Blaabjerg, "Unified impedance model of grid-connected voltage-source converters," *IEEE Trans. Power Electron.*, vol. 33, no. 2, pp. 1775–1787, 2018.

[20] J. Fang, X. Li, H. Li, and Y. Tang, "Stability improvement for three-phase grid-connected converters through impedance reshaping in quadrature-axis," *IEEE Trans. on Power Electron.*, vol. 33, no. 10, pp. 8365-8375, 2017.

[21] N. R. Merritt, C. Chakraborty, and P. Bajpai, "New voltage control strategies for VSC-based DG units in an unbalanced microgrid," *IEEE Trans. on Sustain. Energy,* vol. 8, no. 3, pp. 1127-1139, 2017.

[22] J. He, Y. W. Li, J. M. Guerrero, F. Blaabjerg, and J. C. Vasquez, "An Islanding Microgrid Power Sharing Approach Using Enhanced Virtual Impedance Control Scheme," *IEEE Trans. on Power Electron.*, vol. 28, no. 11, pp. 5272-5282, Nov. 2013.

[23] X. Wang, F. Blaabjerg, and W. Wu, "Modeling and analysis of harmonic stability in an AC power-electronics-based power system," *IEEE Trans. on Power Electron.*, vol. 29, no. 12, pp. 6421-6432, 2014.

[24] B. Mahamedi, M. Eskandari, J. Fletcher, J. Zhu, "Sequence-Based Control Strategy With Current Limiting for the Fault Ride-Through of Inverter-Interfaced Distributed Generators," *IEEE Trans. on Sustain. Energy,* vol. 11, no. 1, pp. 165-174, 2020.

[25] B. Mahamedi, J. G. Zhu, M. Eskandari, L. Li, and A. Mehrizi-Sani, "Analysis of Fault Response of Inverter-Interfaced Distributed Generators in Sequence Networks," in *2018 IEEE Industry Applications Society Annual Meeting (IAS)*, 2018, pp. 1-9: IEEE.

[26] M. C. Chandorkar, D. M. Divan, and R. Adapa, "Control of parallel connected inverters in standalone AC supply systems," *IEEE Trans. Ind. Appl.*, vol. 29, no. 1, pp. 136-143, 1993.

[27] M. Eskandari, L. Li, and M. H. Moradi, P. Siano. F. Blaabjerg, "Active power sharing and frequency restoration in an autonomous networked microgrids," *IEEE Trans. on Power Syst.*, vol. 34, no. 6, pp. 4706-4717, 2019.

[28] H. Han, X. Hou, J. Yang, J. Wu, M. Su, and J. M. Guerrero, "Review of power sharing control strategies for islanding operation of AC microgrids," *IEEE Trans. on Smart Grid,* vol. 7, no. 1, pp. 200-215, 2016.

[29] Y. Han, H. Li, P. Shen, E. A. A. Coelho, and J. M. Guerrero, "Review of active and reactive power sharing strategies in hierarchical controlled microgrids," *IEEE Trans. on Power Electron.*, vol. 32, no. 3, pp. 2427-2451, 2017.

[30] W. Yao, M. Chen, J. Matas, J. M. Guerrero, and Z.-M. Qian, "Design and analysis of the droop control method for parallel inverters

considering the impact of the complex impedance on the power sharing," *IEEE Trans. on Ind. Electron.,* vol. 58, no. 2, pp. 576-588, 2010.

[31] M. Eskandari, L. Li, M. H. Moradi, P. Siano "A Nodal Approach-based State-Space Model of Droop-Based Autonomous Networked Microgrid," *Sustain. Energy, Grids and Networks,* vol. 18, p. 100216, 2019.

[32] Y. Gu, N. Bottrell, and T. C. Green, "Reduced-order models for representing converters in power system studies," *IEEE Trans. on Power Electron.,* vol. 33, no. 4, pp. 3644-3654, 2017.

[33] P. Monshizadeh, N. Monshizadeh, C. De Persis, and A. van der Schaft, "Output impedance diffusion into lossy power lines," *IEEE Trans. on Power Syst.,* vol. 34, no. 3, pp. 1659-1668, 2018.

[34] J. M. Guerrero, L. G. De Vicuna, J. Matas, M. Castilla, J. Miret. "Output impedance design of parallel-connected UPS inverters with wireless load-sharing control." *IEEE Trans. on Ind. Electron.,* vol. 52, no. 4, pp. 1126-1135. 2005.

[35] M. Eskandari and L. Li, "Microgrid operation improvement by adaptive virtual impedance," *IET Renew. Power Gen.,* vol. 13, no. 2, pp. 296-307, 2018.

[36] M. Rasheduzzaman, J. A. Mueller, and J. W. Kimball, "Reduced-order small-signal model of microgrid systems," *IEEE Trans. on Sustain. Energy,* 6(4). 1292-1305, 2015.

[37] M. Eskandari, L. Li, and M. H. Moradi. "Decentralized Optimal Servo Control System for Implementing Instantaneous Reactive Power Sharing in Microgrids." *IEEE Trans. on Sustain. Energy*, vol. 9, no. 2, 525-537, 2018.

[38] X. Wang, Y. W. Li, F. Blaabjerg, and P. C. Loh, "Virtual-impedance-based control for voltage-source and current-source converters," *IEEE Trans. on Power Electron.,* vol. 30, no. 12, pp. 7019-7037, 2014.

[39] M. Eskandari, L. Li, M. H. Moradi, P. Siano, F. Blaabjerg, "Optimal Voltage Regulator for Inverter Interfaced DG Units-Part I: Control System," *IEEE Trans. on Sustain. Energy, 2020.*

[40] J. Huang, K. A. Corzine, and M. Belkhayat, "Small-signal impedance measurement of power-electronics-based AC power systems using line-to-line current injection," *IEEE Trans. on Power Electron.,* vol. 24, no. 2, pp. 445-455, 2009.

[41] J. He, Y. W. Li, and M. S. Munir, "A flexible harmonic control approach through voltage-controlled DG–grid interfacing converters," *IEEE Trans. on Ind. Electron.,* vol. 59, no. 1, pp. 444-455, 2011.

[42] M. Savaghebi, et al., "Secondary control scheme for voltage unbalance compensation in an islanded droop-controlled microgrid," *IEEE Trans. on Smart Grid,* vol. 3, no. 2, pp. 797-807, 2012.